Equation-of-State Parameters for Pure Polymers by Molecular Dynamics Simulations

Maurizio Fermeglia and Sabrina Pricl
Dept. of Chemical, Environmental and Raw Materials Engineering, University of Trieste, I-34127 Trieste, Italy

Two new procedures, based on molecular mechanics and molecular dynamics computer simulations, are presented for estimating the PHSCT EOS and the LF EOS parameters of a set of four polymers of industrial relevance and to predict their PVT behavior. These new, original methods offer good results, are relatively inexpensive, are absolutely general, and can be applied in principle to any equation of state, provided the model parameters have a well-defined physical meaning.

Introduction

Macromolecular chains present a particularly demanding challenge to computer simulation. Unlike their shorter analogs, for which several properties are determined predominantly by short-range interactions and the important fluctuations occur over short times, a full description of amorphous polymers requires considerations of length scales ranging from the size of the monomeric units to the end-to-end distance of the chains. During the last decades, computer experiments based on molecular mechanics (MM) and molecular dynamics (MD) simulation techniques have opened avenues in the calculations and predictions of both equilibrium and nonequilibrium thermophysical properties of small molecules and long polymeric chains as well (Theodorou and Suter, 1985; Rigby and Roe, 1990; Boyd and Krishna Pant, 1991; Colburn, 1994; Vasudevan and McGrath, 1996; Gubbins and Quirke, 1996).

At the same time, however, notwithstanding the extraordinary evolution of computing power, it is not currently possible to perform reliable atomistic MD simulations of polymers containing more than 10^4 atoms for times of the order of nanoseconds, even on powerful workstations. Nevertheless, by trying to make the structural polymer model as realistic as possible, computer simulations can indeed be used to predict molecular properties for which the experimental determination is too costly, time-consuming, or even impossible. A clear illustration of this assertion can be found in the determination of vapor–liquid equilibria for liquid mixtures. If we consider that the approximate number of important chemicals produced by the chemical industry all over the world is of the order of 10^3, we can estimate that the entity of possible binary systems is of the order 5×10^5. Recently, the cost of producing one VLE data point for a binary mixture has been estimated to be about $2600 and to take on average 2 days (Moser and Kistenmacher, 1987; Gubbins, 1994). Therefore, despite the limitations imposed by the computing resources currently available, simulations can still be considered cheaper and faster than real experiments, at least for simple molecules.

Further, from this type of virtual experiment it should be possible, in principle, to extract the characteristic parameters of some equation of state (EOS), thus avoiding tedious experimental efforts for determining pressure–volume–temperature (PVT) isotherms and vapor pressure as a function of temperature.

As an exploratory work to combine molecular-mechanics/molecular-dynamics techniques and the EOS theory, we first developed a strategy to calculate the perturbed hard-sphere chain (PHSCT) EOS parameters A^*, V^*, and E^* and the lattice fluid (LF) EOS parameters P^*, ρ^*, and T^*, and then predicted and compared the PVT behavior of four synthetic polymers of industrial relevance with the available experimental results. In the case of the PHSCT EOS parameters, the proposed method basically consists in the rough estimation of the molecular surface areas and volumes, related to the corresponding EOS parameter A^* and V^*, by a combination of molecular mechanics and graphical algorithms, whereas the third, energetic parameter E^* can be ob-

Correspondence concerning this article should be addressed to S. Pricl.

tained from MD simulations of the appropriate monomers in the gas state. For the LF EOS, the procedure consists of determining PVT data sets via MD simulations at different decreasing temperatures. The two EOS parameters P^* and ρ^* can be directly obtained by data extrapolation to 0 K, whereas the third parameter T^* can be evaluated by inserting P^*, ρ^*, and a set of simulated PVT data into the EOS expression.

Even though specific equations of state have been considered in this work, the proposed procedures hold an absolutely general character and can be applied to any equation of state, provided the pure-component parameters have a sound and well-defined physical meaning. In our opinion, this method could be of great help in integrating molecular dynamics techniques and process simulators, particularly in those cases where EOS parameters must be obtained for molecules with scarce if not absent experimental data sets available.

Simulation Details

All simulations were performed on a Silicon Graphics Origin 200 (microprocessor MIPS RISC 10000, 64-bit CPU, 128 MB RAM). The commercial software *Cerius*[2] (Version 3.8) from Molecular Simulation Inc. was used for both MM and MD simulations. The generation of accurate model amorphous structures of four synthetic polymers of industrial application, that is, poly(epichloridrine) (PECH), poly(ϵ-caprolactone) (PCL), poly(vinylchloride) (PVC), and atactic poly(propylene) (*a*-PP), was conducted as follows. For each polymer, the constitutive repeating unit (CRU) was first built and its geometry optimized by energy minimization using the COMPASS force field (FF). The COMPASS FF is an augmented version of the CFF series of force fields (Maple et al., 1988; Maple et al., 1994a,b; Hwang et al., 1994), and is the first *ab initio* force field that has been parametrized and validated using condensed-phase properties in addition to various *ab initio* and empirical data for molecules in isolation. The bond terms of the COMPASS FF potential energy function include a quartic polynomial both for bond stretching and angle bending, a three term Fourier expansion for torsions and a Wilson out-of-plane coordinate term. Six crossterms up through 3rd order are present to account for coupling between the intramolecular coordinates. The final two nonbonded terms represent the intermolecular electrostatic energy and the van der Waals interactions, respectively; the latter employs an inverse 9th-power term for the repulsive part rather than the more customary 12th-power term (see the Appendix for details).

The monomers were modeled to have a total charge equal to zero, and the distribution of the partial charge within each molecule was determined by the charge equilibration method of Rappé and Goddard (1991). Energy was minimized by up to 5000 Newton-Raphson iterations. Following this procedure, the root-mean-square (rms) atomic derivatives in the low-energy regions were smaller than 0.05 kcal/mole Å. Long-range nonbonded interactions were treated by applying suitable cutoff distances, and to avoid the discontinuities caused by direct cutoffs, the cubic-spline switching method was used (Brooks et al., 1985). Van der Waals distance and energy parameters for nonbonded interactions between heteronuclear atoms were obtained by the 6th-power combination rule proposed by Waldman and Hagler (1993).

For the prediction of the polymeric properties, first each CRU was polymerized to a conventional degree of polymerization (DP) equal to 100. Explicit hydrogens were used in all model systems, thus bringing the total number of atoms in each polymeric chain to 600 in the case of PVC, 900 for *a*-PP, 1,000 for PECH, and 1,800 for PCL, respectively. Six different amorphous structures for each polymeric chain were generated via the rotational isomeric state (RIS) algorithm (Flory, 1974; Mattice and Suter, 1994), at $T = 386$ K, and packed into a cubic simulation box with 3-D periodicity. The initial density for each chain was set equal to the corresponding available literature values, in order to minimize discrepancies in the final density values obtained from MD simulations (Li and Mattice, 1992; Fan et al., 1994). The structures were then relaxed to minimize energy and avoid atom overlaps using the conjugate-gradient method. In each case, the Ewald technique was employed in handling nonbonded interactions and the charge equilibration method was again used to equilibrate the charge distribution.

Such a straightforward molecular mechanics scheme is likely to trap the simulated system in a metastable local high-energy minima. To prevent the system from such entrapments, the relaxed structures were subjected to simulated annealing (five repeated cycles from 386 K to 1,000 K and back) using constant volume/constant temperature (NVT) MD conditions. At the end of each annealing cycle, the structures were again relaxed via FF, using an rms force less than 0.1 kcal/mole Å for the polymer and 0.1 kcal/mole Å^3 for the stresses on the periodic boxes as convergence criteria. Both convergence criteria were simultaneously satisfied for the system to be relaxed completely. The simulation box was allowed to vary in size and shape during energy minimization, in order to find the equilibrium density for each structure. A long single chain instead of many shorter chains was selected for simulation in order to avoid the unusual distribution of free volumes due to several chain ends.

From the fully relaxed models of the corresponding polymeric chains, isothermal-isobaric (NPT) MD experiments were run at 373 K (a temperature above the glass transition temperature for all polymers) and from 350 to 50 K at intervals of 50 K; the information at 0 K, needed for the LF EOS parameters estimation, was then collected by extrapolation. The Newton atomic equations of motion were integrated numerically by the Verlet leapfrog algorithm (Verlet, 1967), using an integration step of 1 fs. For the NPT dynamics simulations, the relaxation time $\tau = 0.1$ ps and a cell mass prefactor for the masslike parameter W equal to 1.00 were used. Temperature was controlled via weak coupling to a temperature bath (Berendsen et al., 1984) with coupling constant $\tau_T = 0.01$ ps, whereas pressure was kept constant by coupling to a pressure bath (Andersen, 1980), with relaxation time $\tau_P = 0.1$ ps. Since the partial charges assigned by the charge equilibration method are dependent on structure geometry, the partial charges were updated regularly every 100 MD steps during the entire MD runs. Each NPT MD run was started by assigning initial velocity for the atoms according to a Boltzmann distribution at $2 \times T$. It consisted in an equilibration phase of 50 ps (that is, 50,000 MD steps with time step = 1 fs), during which system equilibration was monitored by

recording the instantaneous values of the total, potential, and kinetic energy and the time evolution of the volume, and in a data-collection phase, which was extended up to 250 ps.

The estimation of the molecular surface area and volumes, required for the determination of the PHSCT EOS parameters A^* and V^*, was performed via the Connolly dot algorithm (Connolly, 1983a,b, 1985). Accordingly, a probe sphere of a given radius, representing the solvent molecule, is placed tangent to the atoms of the molecule at thousands of different positions. For each position in which the probe does not experience van der Waals overlap with the atoms of the molecule, points lying on the inward-facing surface of the probe sphere become part of the molecule solvent-accessible surface (SAS). According to this procedure, the molecular surface generated consists of the van der Waals surface of the atoms, which can be touched by a solvent-sized probe sphere [thus called contact surface (CS)], connected by a network of concave and saddle surfaces [globally called reentrant surface (RS)] that smoothes over crevices and pits between the atoms of the molecule. The sum of the contact and reentrant surface from the so-called molecular surface (MS); this surface is the boundary of the molecular volume (MV) that the solvent probe is excluded from if it is not to undergo overlaps with the molecule atoms, which therefore is also called solvent-excluded volume (SEV). Finally, performing the same procedure by setting the probe-sphere radius equal to zero, the algorithm yields the van der Waals surface (WS).

Recently, the Connolly algorithm has been proved to be not too accurate for the determination of molecular volumes. Indeed, it had been observed that the molecular volumes derived using algorithms based on van der Waals radii are generally 25% lower than the experimentally determined volumes for polypeptides (Rellick and Becktel, 1997). Nevertheless, to the purpose of our procedure, the values of the molecular surface areas and volumes obtained with this technique are reasonable enough and can be used, without resorting to any correction (Fermeglia and Pricl, 1998), in the calculation of the related EOS parameters.

Theory

The first equation of state considered in this work is based on the simplified PHSCT EOS (Song and Mason, 1991; Song et al., 1994a,b 1996), in which the polymer molecule is considered to be constituted by chains of freely jointed tangent hard spheres. The PHSCT EOS has been developed starting from the modified Chiew equation of state for hard-sphere chains as the reference term (Chiew, 1990), a van der Waals-type perturbation term, and the Song-Mason method to relate equation-of-state parameters to the intermolecular potential (Song and Mason, 1991).

The relevant equation in terms of pressure can be expressed as

$$\frac{P}{\rho kT} = 1 + r^2 b\rho g(d^+) - (r-1)\left[g(d^+) - 1\right] - \frac{r^2 a\rho}{kT}, \quad (1)$$

where P is the pressure, T the absolute temperature, $\rho = N/V$ the number density (with N the number of molecules and V the volume of the system, respectively), k the Boltzmann constant, d^+ the hard-sphere diameter, and $g(d^+)$ the pair distribution function of hard spheres at contact. Three parameters appear in Eq. 1, all characterized by a well-defined physical meaning: the number of effective hard spheres per molecule r, the intermolecular potential-well depth between a nonbonded pair of segments a, and the segmental diameter b.

By defining the polymer segment density ρ_r as

$$\rho_r = r\rho \quad (2)$$

Eq. 1 can be rewritten as

$$\left(\frac{P}{\rho_r kT}\right) = 1 + b\rho_r g(d^+) - \left(1 - \frac{1}{r}\right) g(d^+) - \frac{a\rho_r}{kT}. \quad (3)$$

For polymeric chains, $r \to \infty$ and hence $1 - 1/r \to 1$; accordingly, Eq. 1 can be finally recast as

$$\left(\frac{P}{\rho_r kT}\right) = 1 + b\rho_r g(d^+) - g(d^+) - \frac{a\rho_r}{kT}. \quad (4)$$

To obtain an engineering-oriented equation of state, a redefinition of the EOS parameters has been performed (Song and Mason, 1991; Fermeglia et al., 1997, 1998) as follows. The attractive parameter a and the effective hard-sphere diameter b were recast in terms of constants associated with intermolecular potentials and represented by two functions of temperatures:

$$a(T) = \frac{2\pi}{3}\sigma^3 \epsilon F_a(kT/\epsilon) \quad (5)$$

$$b(T) = \frac{2\pi}{3}\sigma^3 \epsilon F_b(kT/\epsilon), \quad (6)$$

where ϵ and σ are the pair potential parameters: ϵ is the depth of the minimum in the pair potential, and σ is the separation distance between segment centers at this minimum; F_a and F_b are two universal functions given by empirical equations determined from thermodynamic properties of argon and methane over a large range of temperature and density (Song et al., 1996).

In summary, each pure component was characterized by a set of three-segment-based parameters—σ, ϵ, and r—that were combined further to yield three final characteristic molecular parameters reflecting the size, shape, and energetic interactions of the fluids considered as follows. First, a characteristic volume, V^*, was defined as

$$V^* = (\pi/6)\frac{r}{M} M_0 \sigma^3 N_A, \quad (7)$$

where N_A is Avogadro's constant, M is the polymer molecular weight, and M_0 is the CRU molecular weight. Second, a characteristic surface area, A^*, was given as

$$A^* = \pi \frac{r}{M} M_0 \sigma^2 N_A; \quad (8)$$

and, finally, a characteristic "cohesive" energy, E^*, was introduced as

$$E^* = \frac{\epsilon}{k}\frac{r}{M} M_0 R_g, \tag{9}$$

where R_g is the gas constant.

According to the procedure proposed in this article, the three EOS parameters can be estimated as follows: from the values of molecular areas and volumes of both the polymer and the corresponding CRU, calculated via the corrected Connolly algorithm, the relevant r and σ values can be calculated and, hence, V^* and A^* can be obtained by means of Eqs. 7 and 8. The parameter ϵ/k is obtained from MD as the ratio of the equilibrium value of the nonbonded contributions of the potential energy and the kinetic energy of the polymer CRU at the given temperature (in our case, $T = 1028$ K); thus, E^* is easily obtained by Eq. 9. Recently, this procedure was successfully applied to quite different systems, such as refrigerants (Fermeglia and Pricl, 1998).

The lattice fluid theory can be considered a generalization of the classic lattice theory, where vacancies are allowed. The theory gives rise to a compressible equation of state that accounts for lower critical solution temperature behavior, thus justifying thermally induced phase separations (Sanchez and Lacombe, 1976; Sanchez and Panayiotou, 1994). The equation of state is expressed as follows:

$$\left(\frac{\rho}{\rho^*}\right)^2 + \left(\frac{P}{P^*}\right) + \left(\frac{T}{T^*}\right)\left\{\ln\left[1-\left(\frac{\rho}{\rho^*}\right)\right] + \left(1-\frac{1}{r}\right)\left(\frac{\rho}{\rho^*}\right)\right\} = 0 \tag{10}$$

where T^*, P^*, and ρ^* are characteristic parameters and $r \to \infty$ for large polymers; specifically, P^* corresponds to the cohesive energy density at 0 K, and ρ^* is related to the specific volume at 0 K. According to our procedure, both P^* and ρ^* values can be calculated via MD by means of the extrapolation maneuver described in the experimental session. The characteristic temperature T^* is finally obtained by inserting P^*, ρ^*, and a simulated PVT data set in Eq. 10.

Results and Discussion

Six independent structures for each polymer considered in this study were generated according to the procedure just described. The properties reported below are then to be considered as ensemble averaged from the appropriate set of six structures. The equilibration process was followed by monitoring the time evolution of the energies. For all polymers at all temperatures considered, the average total, kinetic, and potential energies have ceased to show a systematic drift and have started to oscillate about steady mean values around 30 ps. Accordingly, simulation runs longer than 250 ps were judged not necessary to enhance data accuracy.

A first check on the degree of relaxation of the generated models can be obtained from an inspection of the values of the internal stress tensors in the simulation boxes. Indeed, the internal stress components σ_{ij}—defined as the first derivative of the potential energy per unit volume with respect to strain—should be close to zero at equilibrium, and any substantial negative or positive deviations suggest the system to be under compression or tension, respectively. As an example, the average values of the on-diagonal terms σ_{ii} of the internal stress tensors (that is, $1/3\ \langle \sigma_{ii} \rangle$, in MPa) in the simulation boxes for all polymers at the end of the equilibration phase at 373 K were 0.72 ± 0.19 for PECH, 0.14 ± 0.18 for PCL, 0.10 ± 0.16 for PVC, and 0.72 ± 0.24 for *a*-PP, respectively. The corresponding average deviatoric part is also small, being equal to 0.18 ± 0.12 for PECH, 0.054 ± 0.044 for PCL, 0.060 ± 0.057 for PVC, and 0.23 ± 0.11 for *a*-PP, respectively. The very low values of the σ_{ij} seem to suggest that the final average polymer structures are well relaxed. Analogous results are obtained at all other temperatures considered.

All simulated structures were in an amorphous state, as confirmed by inspection of the corresponding radial distribution functions (RDF). At long distances (> 5 Å), the RDF for all polymers approach unity, indicating that no long-range structure exists, as one would expect from a purely amorphous system.

Table 1. Ensemble Averaged Molecular Surface Areas and Volumes for the Four CRUs and Corresponding Polymers

Polymer	A_{CRU} (Å^2)	V_{CRU} (Å^3)	A_p (Å^2)	V_p (Å^3)
$a-$PP	90.7 ± 0.2	61.0 ± 0.2	$6{,}406 \pm 15$	$9{,}396 \pm 21$
PVC	84.9 ± 0.2	57.9 ± 0.2	$5{,}815 \pm 12$	$4{,}793 \pm 14$
PECH	106 ± 0.3	76.2 ± 0.3	$9{,}352 \pm 22$	$7{,}404 \pm 39$
PCL	170 ± 0.4	124 ± 0.6	$10{,}112 \pm 34$	$9{,}687 \pm 54$

PHSCT EOS results

According to our procedure, the determination of the two PHSCT EOS parameters V^* and A^* is straightforward. Table 1 shows the ensemble averaged values of the molecular surface areas and volumes for all the polymers and the relevant CRUs, whereas Table 2 reports the corresponding calculated values of the PHSCT EOS parameters.

The *a priori* calculated parameters reported in Table 2 were then inserted in the PHSCT EOS expression and the corresponding thermodynamical properties of the polymers considered have been predicted and compared with the relevant experimental data (Rodgers, 1993). Table 3 reports the results of this comparison in terms of rms deviation (RMSD),

Table 2. Calculated PHSCT EOS Parameters for the Four Polymers

Polymer	A^* (10^{-9} cm^2/mol)	V^* (cm^3/mol)	E^* (bar·dm^3/mol)
$a-$PP	5.45	40.33	52.67
PVC	5.59	32.93	62.35
PECH	6.34	62.32	60.43
PCL	10.2	166.2	80.25

Table 3. Experimental Density Data vs. PHSCT EOS Predictions Using the Parameter Values in Table 2

Polymer	*P* Range (MPa)	*T* Range (K)	RMSD (%)
a−PP	0−196	446.66−571.63	2.5
PVC	0−200	373.35−423.15	1.1
PECH	0−200	333.15−413.15	2.5
PCL	0−200	373.75−421.35	1.7

defined as:

$$\mathrm{RMSD} = 100 \sum_i \sqrt{\frac{\left(M_i^{\exp} - M_i^{\mathrm{calc}}\right)^2}{N\left(M_i^{\exp}\right)^2}}, \qquad (11)$$

where $M_i^{\exp}$ is the experimental value of a generic property M, M_i^{calc} is the corresponding calculated value, and N is the total number of data points, whereas two graphical examples are given by Figure 1a and 1b for *a*-PP and PVC, respectively (only some selected data sets are reported in each Figure part for the sake of clarity). In terms of RMSD, the quality of the results shown in Table 3 and in the pertinent figures is rather good. Nevertheless, the predicted values show, in all cases, a definite trend in the temperature dependence of the thermophysical properties. A cause for this trend can be reasonably ascribed to the oversimplification of the perturbation term in Eq. 4 that includes, with a certain degree of empiricism, both the van der Waals and the electrostatic interactions. This approximation could be accounted for by including a temperature dependence of the EOS parameters or by explicitly adding a term to the EOS expression. Yet, since the purpose of our article is to present and test a new procedure for the generation of EOS parameters rather than validating or proposing a new thermodynamic model, we can consider the global prediction results listed in Table 3 more than satisfactory.

LF EOS

Table 4 reports the ensemble averaged energies of the equilibrated amorphous polymeric structures, the averaged PVT data at all simulated temperatures, and the corresponding values extrapolated to 0 K. The small deviations in the energy components and their sum for all polymers are again an indication of the good structure equilibration. The kinetic energy value extrapolated at 0 K is practically 0, which is quite sensible since any thermal motion vanishes at 0 K. Accordingly, under these conditions, $E_{\mathrm{pot}} = E_{\mathrm{tot}}$.

As briefly mentioned in the theory section, the LF EOS parameter P^* directly corresponds to the cohesive energy density at 0 K, e_{coh}^0. In general, e_{coh} is defined as the ratio of the cohesive energy E_{coh} and the molar volume V at a given temperature; E_{coh}, in turn, is defined as the increase in internal energy per mole of substance if all intermolecular forces are eliminated. In our simulated systems, each chain is surrounded by other chains that are simply displaced images of the chain itself. The cohesive energy is the energy of interactions between these images. Accordingly, the values of E_{coh} at different temperatures can be obtained from simulation by calculating the difference between the nonbonded energy of the periodic structure $E_{nb}^{periodic}$ and the corresponding value for an isolated parent chain *in vacuum* $E_{nb}^{isolated}$:

$$E_{\mathrm{coh}} = E_{nb}^{\mathrm{isolated}} - E_{nb}^{\mathrm{periodic}}. \qquad (12)$$

Finally, the value of E_{coh} at 0 K can be gained by extrapolation.

To this end, six parent chains for each polymer were generated and their energy minimized according to the procedure described in the simulation details section. The simulated annealing method was again applied to these systems as described earlier, to provide thermal energies to cross energy barriers between conformation local minima. Finally, NVT MD simulations were performed on the single chains (again the six best relaxed chains for each polymer) *in vacuum* at the same temperature conditions applied for the simulations

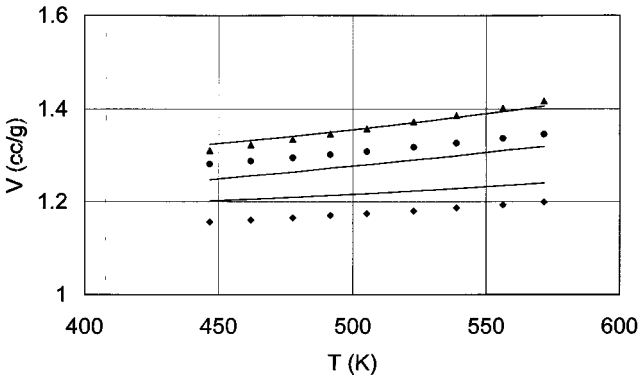

Figure 1a. Experimental (symbols) PVT behavior of *a*-PP vs. corresponding predictions (lines) obtained with the PHSCT EOS using the parameter values in Table 2.

▲, $P = 0$ bar; ●, $P = 490$ bar; ♦, $P = 1{,}960$ bar

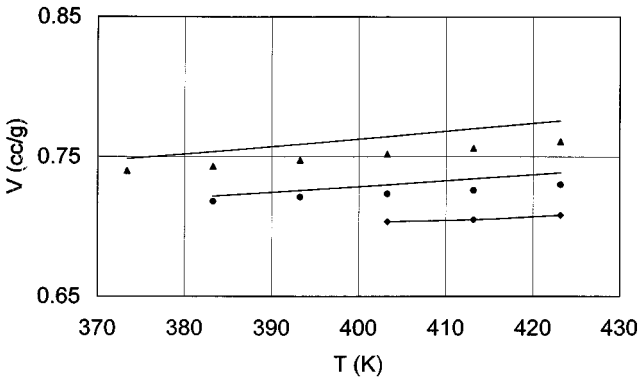

Figure 1b. Experimental (symbols) PVT behavior of PVC vs. corresponding predictions (lines) obtained with the PHSCT EOS using the parameter values in Table 2.

▲, $P = 0$ bar; ●, $P = 800$ bar; ♦, $P = 1{,}700$ bar.

Table 4. Ensemble Averaged Energies, Simulated PVT Data and Corresponding Values Extrapolated to 0 K

T (K)	E_{tot} (kcal/mol)	E_{pot} (kcal/mol)	E_{kin} (kcal/mol)	E_{nb} (kcal/mol)	E_{val} (kcal/mol)	E_{ct} (kcal/mol)	P (MPa)	d (g/cm^3)
Equilibrated PECH								
386	465.8 ± 7.61	−686.4 ± 23.3	1,152 ± 21.7	−1,250 ± 19.3	783.9 ± 29.6	−220.2 ± 4.9	4.4	1.297 ± 0.004
353	285.7 ± 4.35	−768.9 ± 16.7	1,055 ± 15.2	−1,259 ± 13.6	697.7 ± 18.5	−207.6 ± 8.3	4.1	1.320 ± 0.002
296	−28.63 ± 7.22	−913.0 ± 14.1	884.3 ± 10.3	−1,274 ± 15.4	547.3 ± 11.4	−186.3 ± 3.8	4.4	1.341 ± 0.005
257	−244.7 ± 8.15	−1,012 ± 18.2	767.3 ± 8.4	−1,284 ± 18.9	443.9 ± 7.0	−171.9 ± 6.3	2.5	1.355 ± 0.002
210	−503.0 ± 3.66	−1,130 ± 16.2	627.3 ± 9.1	−1,296 ± 19.2	320.1 ± 8.3	−154.1 ± 3.8	4.3	1.378 ± 0.004
151	−828.5 ± 4.89	−1,280 ± 14.9	451.0 ± 5.6	−1,311 ± 16.6	164.5 ± 7.8	−133.5 ± 4.1	4.2	1.396 ± 0.003
100	−1,109 ± 3.11	−1,408 ± 17.6	299.1 ± 2.9	−1,324 ± 11.4	30.37 ± 4.3	−114.4 ± 3.1	3.2	1.411 ± 0.003
51	−1,378 ± 4.62	−1,531 ± 12.4	153.2 ± 2.0	−1,337 ± 16.3	−98.51 ± 5.2	−95.50 ± 4.5	1.3	1.426 ± 0.002
0	−1,661	−1,661	0.00	−1,350	−233.9	−77.10	—	1.441
Equilibrated PCL								
387	1977 ± 10.33	−101.1 ± 20.1	2,078 ± 28.3	−1,002 ± 20.4	1,087 ± 33.9	−186.4 ± 7.4	8.6	1.032 ± 0.004
369	1850 ± 8.12	−133.0 ± 18.1	1,983 ± 26.6	−974.9 ± 18.7	1,022 ± 33.2	−179.9 ± 5.2	1.4	1.040 ± 0.005
301	1362 ± 7.44	−254.2 ± 17.9	1,618 ± 25.5	−873.9 ± 16.5	776.6 ± 25.4	−156.9 ± 6.0	2.3	1.078 ± 0.004
259	1062 ± 6.21	−328.8 ± 15.3	1,392 ± 21.2	−811.5 ± 15.9	625.1 ± 22.2	−142.4 ± 5.5	3.3	1.090 ± 0.003
200	640.0 ± 5.45	−434.0 ± 14.1	1,075 ± 18.3	−723.9 ± 15.1	412.2 ± 20.8	−122.3 ± 4.33	1.5	1.108 ± 0.002
153	303.9 ± 4.89	−517.7 ± 13.6	822.2 ± 15.1	−654.1 ± 14.9	242.6 ± 13.1	−106.2 ± 4.00	4.3	1.122 ± 0.003
101	−67.85 ± 5.22	−610.2 ± 13.2	542.8 ± 12.2	−576.8 ± 13.6	55.01 ± 5.8	−88.42 ± 2.65	3.3	1.138 ± 0.002
52	−418.2 ± 3.11	−697.4 ± 11.0	279.4 ± 6.66	−504.0 ± 12.8	−121.8 ± 10.3	−71.64 ± 2.36	2.1	1.154 ± 0.002
0	−790.0	−790.0	0.00	−426.8	−309.4	−53.83	—	1.168
Equilibrated PVC								
384	178.4 ± 5.45	−526.6 ± 17.5	688.1 ± 15.0	−870.5 ± 10.8	366.2 ± 13.8	−2.960 ± 1.22	2.3	1.348 ± 0.003
367	123.2 ± 4.21	−534.6 ± 12.6	657.8 ± 15.3	−875.9 ± 10.4	352.7 ± 13.3	−11.37 ± 1.32	1.4	1.360 ± 0.004
294	−107.2 ± 2.85	−663.9 ± 13.0	526.7 ± 12.6	−901.1 ± 9.48	289.7 ± 15.5	−52.52 ± 1.12	1.2	1.383 ± 0.002
248	−251.3 ± 2.44	−706.6 ± 10.8	444.4 ± 11.3	−917.4 ± 9.22	249.3 ± 12.8	−79.12 ± 2.09	1.2	1.410 ± 0.005
200	−403.0 ± 3.21	−770.2 ± 9.85	358.4 ± 8.99	−934.0 ± 8.92	208.0 ± 10.3	−106.0 ± 2.00	1.5	1.424 ± 0.002
153	−551.5 ± 2.98	832.4 ± 9.00	274.2 ± 4.67	−950.2 ± 7.32	167.6 ± 8.66	−132.3 ± 1.98	2.1	1.437 ± 0.003
99	−722.2 ± 2.09	−903.9 ± 6.48	177.4 ± 3.22	−968.8 ± 7.20	121.1 ± 6.73	−162.6 ± 1.44	1.8	1.452 ± 0.001
52	−870.7 ± 2.88	−966.2 ± 6.32	93.18 ± 2.13	−985.1 ± 5.98	80.72 ± 5.23	−188.9 ± 1.56	1.1	1.463 ± 0.003
0	1035	1035	0.00	−1,003	35.97	−218.0	—	1.471
Equilibrated a − PP								
366	1,340 ± 2.15	355.6 ± 5.2	984.0 ± 19.7	−20.13 ± 1.17	452.8 ± 13.15	−77.02 ± 4.71	2.5	0.821 ± 0.005
345	1,227 ± 1.85	299.2 ± 3.98	928.1 ± 11.4	−24.93 ± 1.13	398.8 ± 11.16	−74.62 ± 3.67	1.6	0.834 ± 0.003
292	937.0 ± 1.33	152.7 ± 2.33	784.3 ± 7.55	−36.87 ± 1.15	264.0 ± 9.89	−74.43 ± 3.55	1.8	0.858 ± 0.003
255	736.6 ± 2.01	50.80 ± 2.52	686.0 ± 5.67	−45.27 ± 1.13	169.3 ± 6.62	−73.18 ± 3.02	1.4	0.862 ± 0.002
209	485.9 ± 2.09	−76.16 ± 1.25	562.2 ± 4.88	−55.67 ± 1.12	51.95 ± 4.22	−72.44 ± 3.67	1.5	0.876 ± 0.004
154	186.1 ± 1.11	−228.0 ± 2.05	414.3 ± 4.01	−68.10 ± 1.08	−88.30 ± 3.09	−71.56 ± 2.19	1.5	0.892 ± 0.001
101	−102.8 ± 3.32	−374.2 ± 1.69	271.7 ± 3.09	−80.07 ± 1.05	−223.5 ± 2.03	−70.72 ± 3.44	1.3	0.907 ± 0.003
52	−369.8 ± 2.15	−509.5 ± 1.88	139.9 ± 3.00	−91.15 ± 1.00	−384.4 ± 1.33	−69.93 ± 2.10	1.2	0.920 ± 0.002
0	−653.2	−653.2	0.00	−102.93	−481.0	−69.27	—	0.9337

of the relevant periodic systems. For example, Table 5 reports the comparison between the energy components of PECH and its parent chain at 386 K. As expected, the valence contribution to E_{tot} is nearly the same for both chains, and the major difference is indeed given by the nonbonded term $E_{nb} = E_{vdw} + E_{coul}$. As a matter of fact, it can be easily understood that the reduction in the total energy for the chain in bulk rises solely due to the intermolecular nonbonded attractive interactions between the atoms from neighboring chains.

Table 5. Energy Components of PECH vs. Its Parent Chain at 386 K

Energy (kcal/mol)	PECH	PECH Parent Chain
E_{tot}	465.8 ± 7.61	1,069 ± 10.4
E_{pot}	−686.4 ± 23.3	−79.79 ± 5.85
E_{kin}	1,152 ± 21.7	1,148 ± 20.9
E_{nb}	−1,250 ± 19.3	−627.3 ± 15.0
E_{vdw}	−290.9 ± 16.0	−49.20 ± 4.02
E_{coul}	−959.5 ± 12.8	−578.1 ± 9.47
E_{val}	783.9 ± 29.6	744.9 ± 29.2
E_{bond}	442.8 ± 18.3	441.0 ± 17.8
E_{angle}	885.3 ± 25.1	860.1 ± 25.8
E_{tors}	−544.2 ± 9.58	−556.2 ± 7.86
E_{ct}	−219.9 ± 11.3	−197.4 ± 10.2

A further check on data accuracy can be performed at this point. Since the Hildebrand solubility parameter δ (Hildebrand and Scott, 1949) is simply defined as the square root of e_{coh}, we calculated the values of δ at 298 K and compared them with the available data in the literature (van

Table 6. Experimental Solubility Parameters vs. Values Obtained by MD Simulations for All Polymers at 298 K

Polymer	δ_{calc} (J/cm^3)$^{1/2}$	δ_{exp} (J/cm^3)$^{1/2}$
PECH	19.9	19.2
PCL	20.2	—
PVC	19.6	19.2−22.1
a − PP	16.8	16.8−18.8

Table 7. Calculated LF EOS Parameters for the Four Polymers

Polymer	P^* (MPa)	ρ^* (g/cm^3)	T^* (K)
PECH	446.2	1.441	662
PCL	476.0	1.168	613
PVC	463	1.471	711
a-PP	332.0	0.9337	578

Krevelen, 1990). Table 6 shows that the agreement between the theoretical prediction and experiment is excellent.

Accordingly, in Table 7 we report the values of the three LF EOS parameters for all polymers. For each macromolecule, P^* is equal to e^0_{coh} obtained by extrapolation as explained earlier, ρ^* is the polymer density value at 0 K (see Table 4), and T^* is obtained by inserting the corresponding P^*, ρ^*, and the simulated P and ρ values at the highest simulated temperatures (see Table 4) in Eq. 10.

The PVT data for all polymers were then predicted with Eq. 10 using the appropriate parameter sets listed in Table 7. Figures 2a and 2b are two selected examples of the comparison between the predicted and the corresponding available experimental values (Rodgers, 1993). It may be seen that the agreement between the relevant data sets is more than satisfactory in all cases. To quantify the quality of our PVT predictions, in this case we calculated the percent relative average deviations (%RAD), defined as

$$\%\mathrm{RAD} = 100 \times \frac{1}{N} \sum_i \frac{|M_i^{\exp} - M_i^{\mathrm{calc}}|}{M_i^{\mathrm{calc}}}, \qquad (13)$$

where again N is the number of data points, $M_i^{\exp}$ is the experimental value, and M_i^{calc} is the corresponding calculated value. The values of %RAD averaged over the entire P/T range for each polymer are shown in Table 8, where we also report the %RAD obtained by using Eq. 10 with two

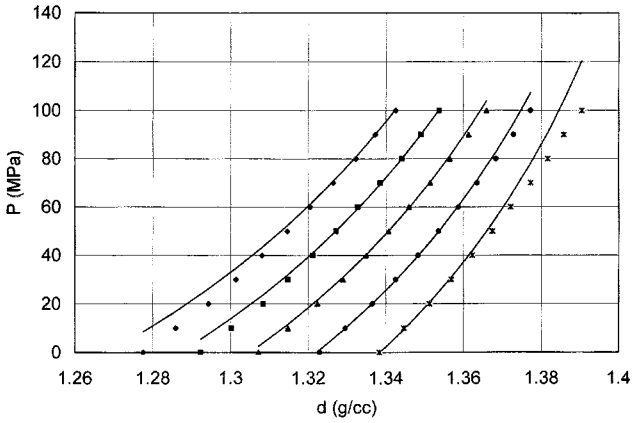

Figure 2a. Experimental (symbols) PVT behavior of PECH vs. corresponding predictions (lines) obtained with the LF EOS using the parameter values in Table 7.

∗, T = 333.15 K; ●, T = 353.15 K; ▲, T = 373.15 K; ■, T = 393.15 K; ♦, T = 413.15 K.

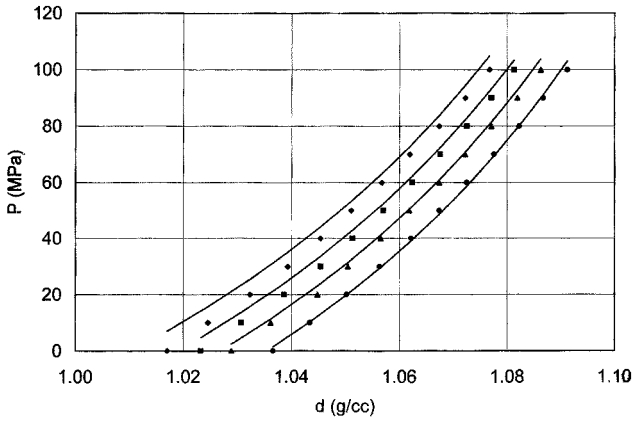

Figure 2b. Experimental (symbols) PVT behavior of PCL vs. corresponding predictions (lines) obtained with the LF EOS using the parameter values in Table 7.

●, T = 373.15 K; ▲, T = 384.05 K; ■, T = 393.35 K; ♦, T = 403.26 K.

other parameter sets that are available in the literature (Rodgers, 1993; Sanchez and Panayiotou, 1994). From an inspection of this table, we can not only conclude that the proposed procedure is indeed useful for the determination of the LF EOS parameters but also that the PVT data prediction quality thus obtained is comparable, if not superior, to that obtainable with the current literature parameter values.

Conclusions

This article reports the results obtained with two new procedures for estimating EOS parameters from computer simulations. The problem of estimating reasonable parameters for EOS is a topical issue in the analysis and synthesis of chemical processes and in the use of process simulators. In this last case, for instance, chemical engineers need to input EOS parameters for small molecules that have not yet been synthesized, or for long-chain polymers for which experimental data cannot be easily obtained (due to peculiar process or experimental conditions). Furthermore, in the calculation of rate-controlled processes, it is sometimes necessary to estimate the equilibrium condition with a high degree of accuracy, and again experimental data in such conditions may not be available.

The new, original methods proposed in this work give good results, are relatively inexpensive, absolutely general, and can

Table 8. RAD: Experimental Density Data vs. LF EOS Predictions Using the Parameter Values in Table 7

Polymer	P Range (MPa)	T Range (°C)	RAD (%)	RAD (Rodgers, 1993) (%)	RAD (Sanchez and Panayiotou, 1994) (%)
PECH	0–100	60.0–140.0	7	23	24
PCL	0–100	100.6–148.2	5	9	10
PVC	0–100	100.2–150.0	7	20	7
a–PP	0–100	80.0–120.0	5	8	7

be applied in principle to any EOS, provided the parameters have a well-defined physical meaning. The tuning of one EOS parameter to a generated datum accounts for the degree of empiricism introduced at a certain stage in the development of any EOS. Further work is in progress to extend the method to other EOSs and to enlarge the database test substances.

Acknowledgments

The authors thank the Ministero dell'Università e della Ricerca Scientifica MURST-Roma) and the University of Trieste (special grant for Scientific Research) for the financial support.

Notation

A_{CRU} = monomer molecular surface area
A_p = polymer molecular surface area
d = density
E_{coul} = electrostatic energy of a system
E_{ct} = cross-term energy of a system
E_{kin} = kinetic energy of a system
$E_{\rm pot}$ = potential energy of a system
$E_{\rm tot}$ = total energy of a system
$E_{\rm val}$ = valence energy of a system
E_{vdw} = Lennard-Jones interaction energy of a system
$g(r)$ = radial distribution function
V_{CRU} = monomer molecular volume
V_p = polymer molecular volume

Literature Cited

Andersen, H. C., "Molecular Dynamics Simulations at Constant Pressure and/or Temperature," *J. Chem. Phys.*, **72**, 2384 (1980).
Berendsen, H. J. C., J. P. M. Postma, W. F. van Gunsteren, A. DiNola, and J. R. Haak, "Molecular Dynamics with Coupling to an External Bath," *J. Chem. Phys.*, **81**, 3684 (1984).
Boyd, R. H., and P. V. Krishna Pant, "Simulation of Glassy Polymethylene Starting from the Equilibrated Liquid," *Macromol.*, **24**, 4078 (1991).
Brooks, C. L., III, R. Montgomery, B. Pettitt, and M. Karplus, "Structural and Energetic Effects of Truncating Long Ranged Interactions in Ionic and Polar Fluids," *J. Chem. Phys.*, **83**, 5897 (1985).
Chiew, Y. C., "Percus-Yevick Integral Equation Theory for Athermal Hard-Sphere Chains. Part I: Equations of State," *Mol. Phys.*, **70**, 129 (1990).
Colburn, E. A., ed., *Computer Simulation of Polymers*, Longman, Harlow, UK (1994).
Connolly, M. L., "Analytical Molecular Surface Calculation," *J. Appl. Crystallog.*, **16**, 548 (1983a).
Connolly, M. L., "Solvent-Accessible Surfaces of Proteins and Nucleic Acids," *Science*, **221**, 709 (1983b).
Connolly, M. L., "Computation of Molecular Volume," *J. Amer. Chem. Soc.*, **107**, 1118 (1985).
Fan, C. F., T. Cagin, Z. M. Chen, and K. A. Smith, "Molecular Modeling of Polycarbonate. 1. Force Field, Static Structure, and Mechanical Properties," *Macromol.*, **27**, 2383 (1994).
Fermeglia, M., A. Bertucco, and D. Patrizio, "Thermodynamic Properties of Pure Hydrofluorocarbons by a Perturbed Hard-Sphere-Chain Equation of State," *Chem. Eng. Sci.*, **52**, 1517 (1997).
Fermeglia, M., A. Bertucco, and S. Bruni, "A Perturbed Hard Sphere Chain Equation of State for Application to Hydrofluorocarbons, Hydrocarbons and Their Mixtures," *Chem. Eng. Sci.*, **53**, 3117 (1998).
Fermeglia, M., and S. Pricl, "Molecular Dynamics Simulations of Real Systems: Application to Chloro-Fluoro-Hydrocarbons and Polymers," *Fluid Phase Equilibria*, **158**, 49 (1999).
Flory, P. J., *Principles of Polymer Chemistry*, Cornell Univ. Press, Ithaca, NY (1974).
Gubbins, K. E., and N. Quirke, eds., *Molecular Simulations and Industrial Applications*, Gordon & Breach, Amsterdam (1996).
Hildebrand, J. H., and R. Scott, *Solubility of Non-Electrolytes*, 3rd ed., Reinhold, New York (1949).
Li, Y., and W. L. Mattice, "Atom Based Modeling of Amorphous 1,4-cis-Butadiene," *Macromolcules*, **25**, 4942 (1992).
Maple, J. R., U. Dinur, and A. T. Hagler, "Derivation of Force Fields for Molecular Mechanics and Dynamics from *ab initio* Energy Surfaces," *Proc. Natl. Acad. Sci. USA*, **85**, 5350 (1988).
Maple, J. R., M.-J. Hwang, T. P. Stockfisch, U. Dinur, M. Waldman, C. S. Ewig, and A. T. Hagler, "Derivation of Class II Force Fields. 1. Methodology and Quantum Force Field for the Alkyl Functional Group and Alkane Molecules," *J. Comput. Chem.*, **15**, 162 (1994a).
Maple, J. R., M.-J. Hwang, T. P. Stockfisch, and A. T. Hagler, "Derivation of Class II Force Fields. 3. Characterization of a Quantum Force Field for Alkanes," *Israel J. Chem.*, **34**, 195 (1994b).
Mattice, W. L., and U. W. Suter, *Conformational Theory of Large Molecules: The Rotational Isomeric State Model in Macromolecular Systems*, Wiley, New York (1994).
Moser, B., and H. Kistenmacher, "An Analysis of the Industrial Use of a Phase Equilibria Prediction Model Based on Thermodynamic Perturbation Theory," *Fluid Phase Equilibria*, **34**, 189 (1987).
Rappé, A. K., and W. A. Goddard III, "Charge Equilibration for Molecular Dynamics Simulations," *J. Phys. Chem.*, **95**, 3358 (1991).
Rellick, L. M., and W. J. Becktel, "Comparison of van der Waals and Semiempirical Calculations of the Molecular Volumes of Small Molecules and Proteins," *Biopolymers*, **42**, 191 (1997).
Rigby, D., and R. J. Roe, "Molecular Dynamics Simulations of Polymer Liquid and Glass. Free-volume Distribution," *Macromol.*, **23**, 5312 (1990).
Rodgers, P. A., "Pressure-Volume-Temperature Relationships for Polymeric Liquids: A Review of Equations of State and Their Characteristic Parameters for 56 Polymers," *J. Appl. Poly. Sci.*, **48**, 1061 (1993).
Sanchez, I. C., and R. H. Lacombe, "An Elementary Molecular Theory of Classical Fluids. Pure Fluids," *J. Phys. Chem.*, **80**, 2352 (1976).
Sanchez, I. C., and C. G. Panayiotou, "Equation of State Thermodynamics of Polymer and Related Solution," *Models for Thermodynamics and Phase Equilibria Calculations*, S. I. Sandler, ed., Dekker, New York, p. 187 (1994).
Song, Y., and E. A. Mason, "Statistical-Mechanical Theory of a New Analytical Equation of State," *J. Chem. Phys.*, **12**, 7840 (1991).
Song, Y., S. M. Lambert, and J. M. Prausnitz, "A Perturbed Hard-Sphere-Chain Equation of State for Normal Fluids and Polymers," *Ind. Eng. Chem. Res.*, **33**, 1047 (1994a).
Song, Y., S. M. Lambert, and J. M. Prausnitz, "Liquid-Liquid Phase Diagram for Binary Polymer Solutions from a Perturbed Hard-Sphere-Chain Equation of State," *Chem. Eng. Sci.*, **17**, 2765 (1994b).
Song, Y., T. Hino, S. M. Lambert, and J. M. Prausnitz, "Liquid-Liquid Equilibria for Polymer Solutions and Blends, Including Copolymers," *Fluid Phase Equil.*, **117**, 69 (1996).
Theodorou, D. N., and U. W. Suter, "Detailed Molecular Structure of a Vinyl Polymer Glass," *Macromol.*, **18**, 1467 (1985).
van Krevelen, D. W., *Properties of Polymers: Their Correlation with Chemical Structure, Their Numerical Estimation and Prediction from Additive Group Contributions*, Elsevier, Amsterdam (1990).
Vasudevan, V. J., and J. E. McGrath, "Atomistic Modeling of Amorphous Aromatic Polybenzoxazoles," *Macromol.*, **29**, 637 (1996).
Verlet, L., "Computer Experiments on Classical Fluids I. Thermodynamical Properties of Lennard-Jones Molecules," *Phys. Rev.*, **159**, 98 (1967).
Waldman, M., and A. T. Hagler, "New Combining Rules for Rare Gas van der Waals Parameters," *J. Comput. Chem.*, **14**, 1077 (1993).

Appendix

The total potential energy E_{pot} of the COMPASS force field is expressed as a combination of valence terms, including diagonal and off-diagonal cross-coupling terms, and nonbonded interaction terms. The analytical form of E_{pot} can

then be written as:

$$E_{pot} = \sum_b \left[K_2(b-b_0)^2 + K_3(b-b_0)^3 + K_4(b-b_0)^4 \right]$$
$$+ \sum_\theta \left[H_2(\theta-\theta_0)^2 + H_3(\theta-\theta_0)^3 + H_4(\theta-\theta_0)^4 \right]$$
$$+ \sum_\phi \left\{ V_1\left[1-\cos\left(\phi-\phi_1^0\right)\right] + V_2\left[1-\cos\left(2\phi-\phi_2^0\right)\right] \right.$$
$$\left. + V_3\left[1-\cos\left(3\phi-\phi_3^0\right)\right] \right\}$$
$$+ \sum_\chi K_\chi \chi^2 \sum_b \sum_{b'} F_{bb'}(b-b_0)(b'-b_0')$$
$$+ \sum_\theta \sum_{\theta'} F_{\theta\theta'}(\theta-\theta_0)(\theta'-\theta_0') + \sum_b \sum_\theta F_{b\theta}(b-b_0)(\theta-\theta_0)$$
$$+ \sum_b \sum_\phi (b-b_0)(V_1\cos\phi + V_2\cos 2\phi + V_3\cos 3\phi)$$
$$+ \sum_{b'} \sum_\phi (b'-b_0')(V_1\cos\phi + V_2\cos 2\phi + V_3\cos 3\phi)$$
$$\sum_\theta \sum_\phi (\theta-\theta_0)(V_1\cos\phi + V_2\cos 2\phi + V_3\cos 3\phi)$$
$$+ \sum_\phi \sum_\theta \sum_{\theta'} K_{\phi\theta\theta'}\cos\phi(\theta-\theta_0)(\theta'-\theta_0')$$
$$+ \sum_{i>j} \frac{q_i q_j}{r_{ij}} + \sum_{i>j} E_{ij}\left[2\left(\frac{r_{ij}^0}{r_{ij}}\right)^9 - 3\left(\frac{r_{ij}^0}{r_{ij}}\right)^6 \right].$$

Manuscript received Mar. 1, 1999, and revision received July 6, 1999.